ADVANCES IN ATMOSPHERIC SCIENCES, VOL. 35, JANUARY 2018, 85–94

• **Original Paper** •

Role of Extratropical Cyclones in the Recently Observed Increase in Poleward Moisture Transport into the Arctic Ocean

Gian A. VILLAMIL-OTERO*[1], Jing ZHANG[1,2], Juanxiong HE[3], and Xiangdong ZHANG[4]

[1]*Department of Physics, North Carolina A&T State University, Greensboro, North Carolina* 27401*, USA*

[2]*Department of Energy and Environmental Systems, North Carolina A&T State University, Greensboro, North Carolina* 27401*, USA*

[3]*Institute of Atmospheric Physics, Chinese Academy of Sciences, Beijing* 100029*, China*

[4]*Department of Atmospheric Science, University of Alaska Fairbanks, Fairbanks, Alaska* 99775*, USA*

(Received 5 May 2017; revised 14 October 2017; accepted 17 October 2017)

ABSTRACT

Poleward atmospheric moisture transport (AMT) into the Arctic Ocean can change atmospheric moisture or water vapor content and cause cloud formation and redistribution, which may change downward longwave radiation and, in turn, surface energy budgets, air temperatures, and sea-ice production and melt. In this study, we found a consistently enhanced poleward AMT across 60°N since 1959 based on the NCAR–NCEP reanalysis. Regional analysis demonstrates that the poleward AMT predominantly occurs over the North Atlantic and North Pacific regions, contributing about 57% and 32%, respectively, to the total transport. To improve our understanding of the driving force for this enhanced poleward AMT, we explored the role that extratropical cyclone activity may play. Climatologically, about 207 extratropical cyclones move across 60°N into the Arctic Ocean each year, among which about 66 (32% of the total) and 47 (23%) originate from the North Atlantic and North Pacific Ocean, respectively. When analyzing the linear trends of the time series constructed by using a 20-year running window, we found a positive correlation of 0.70 between poleward yearly AMT and the integrated cyclone activity index (measurement of cyclone intensity, number, and duration). This shows the consistent multidecadal changes between these two parameters and may suggest cyclone activity plays a driving role in the enhanced poleward AMT. Furthermore, a composite analysis indicates that intensification and poleward extension of the Icelandic low and accompanying strengthened cyclone activity play an important role in enhancing poleward AMT over the North Atlantic region.

Key words: atmospheric moisture transport, cyclone activity, atmospheric circulation, Arctic, climate change

Citation: Villamil-Otero, G. A., J. Zhang, J. X. He, and X. Zhang, 2018: Role of extratropical cyclones in the recently observed increase in poleward moisture transport into the Arctic Ocean. *Adv. Atmos. Sci.*, **35**(1), 85–94, https://doi.org/10.1007/s00376-017-7116-0.

1. Introduction

Alteration of poleward atmospheric moisture transport (AMT) into the Arctic may have significant impacts on Arctic climate changes since moisture, or water vapor, represents one of the major greenhouse gases and critically determines cloud formation and distribution. Increased moisture transport into the Arctic Ocean may, therefore, enhance water-vapor- or cloud-forced downward longwave radiation, contributing to an increase in surface air temperature and summer sea-ice melt and a decrease in winter sea-ice production. Wang and Key (2005) found that increased water vapor content appears to be influential in the enhancement of downward longwave radiation in the Arctic, and Zuidema et al. (2005) further emphasized the role of liquid-water-containing clouds. Francis and Hunter (2006) suggested that the location of the summer ice edge is strongly correlated to the variability in longwave energy emitted by the atmosphere. Kay et al. (2008) found that changes in clouds are an increasingly important control in sea-ice extent minima. In particular, when studying the extreme event of Arctic sea-ice loss in 2007, Kay and Gettelman (2009) found that, while summer cloud reductions enhanced ice-albedo feedback, an increase in cloudiness in fall over newly open water helps trap heat by increasing the downwelling longwave radiation but also reduces net absorbed shortwave radiation. In addition, climate model projections have shown that an increase in poleward AMT caused by a warming planet likely creates a positive feedback on the Arctic system by increasing latent heat release and the emission of longwave radiation to the surface (Skific et al., 2009).

The impact of intense poleward AMT across 70°N during boreal winter on the Arctic-mean downward longwave radi-

* Corresponding author: Gian VILLAMIL-OTERO
Email: gavillam@ncat.edu

ation was recently quantified by Woods et al. (2013). They found that poleward moisture intrusions contribute to about 40% of the interannual variance in downward longwave radiation and about 30% of the interannual variance in skin temperature. Further evidence shows that the increase in downward longwave radiation associated with these moisture intrusions can impact the loss of sea ice (Woods and Caballero, 2016) and result in rapid surface air temperature increases (Kim et al., 2017). Liu and Barnes (2015) investigated these extreme moisture intrusions and found that they are linked to Rossby wave breaking. These planetary-scale waves are capable of diverting moisture, sensible, and latent heat fluxes into the Arctic, enhancing the downward infrared radiation and surface warming (Baggett et al., 2016; Baggett and Lee, 2017; Gong et al., 2017). These moisture intrusions also resemble atmospheric rivers (ARs; Newell et al., 1992; Ralph and Dettinger, 2011; Newman et al., 2012; Liu and Barnes, 2015; Baggett et al., 2016). ARs have been found to account for the majority of poleward moisture transport in the midlatitudes (Zhu and Newell, 1998; Guan and Waliser, 2015). Also, Dacre et al. (2015) attributed the moisture in ARs to local evaporation and convergence within the warm sectors of cyclones, instead of long-range transport as the source.

Synoptic cyclones constitute the major part of atmospheric transient eddies, which may also play an important role in moisture transport, in addition to the stationary and planetary waves (e.g., Peixoto and Oort, 1992; Baggett et al., 2016; Vihma et al., 2016; Baggett and Lee, 2017). Groves and Francis (2002) found that the movement of transient features into the Arctic account for 74% of the net precipitation in the Arctic basin. On the other hand, studies have suggested that cyclone activity plays a key role in the interaction between the surface and the atmosphere and has strong impacts on the Arctic sea ice (Murray and Simmonds, 1995; Sorteberg and Kvingedal, 2006). The strength, rather than the number, of cyclones in the Arctic basin, plays a more critical role in the decrease in September ice extent (Simmonds and Keay, 2009). The impacts of cyclones on the surface and sea ice may be affected through changes in atmospheric moisture content and resulting longwave radiation. In particular, it has been found that cyclone tracks have shifted poleward and cyclone activity has intensified in the Arctic (Zhang et al., 2004; Simmonds et al., 2008; Sepp and Jaagus, 2011; Bender et al., 2012), and the poleward shift may continue in the future as projected by climate models under global warming scenarios (Yin, 2005). So, to improve our understanding of the changes in Arctic atmospheric moisture and the water cycle, we decided to quantitatively investigate the linkages between poleward AMT and extratropical cyclone activity. In this study, we used 60°N as the boundary between the midlatitudes and the Arctic to investigate the impact of extratropical cyclones that move into the Arctic on the AMT. The 60°N line stands as the division between the "polar cap" and the midlatitudes, as it generally corresponds to the zero contour between the polar and midlatitude centers of action of the Arctic Oscillation (AO) (Thompson and Wallace, 1998).

The goal of this study is to understand the role that extratropical cyclone activity plays in the poleward AMT. We seek to achieve this goal by answering the following specific questions: First, do AMT and cyclone activity exhibit any similar regional and interannual variations? Second, which components (e.g., intensity, number, etc.) of cyclone activity correlate closely with the changes in poleward AMT? And finally, how does cyclone activity behave differently under the positive and negative phases of poleward AMT, and how does this difference impact the AMT? The paper is organized as follows: Section 2 describes the data and methods used to obtain the AMT and cyclone activity data. Sections 3 and 4 describe the results of the time series analysis of AMT and cyclone activity and the analysis of the relationship between them. Section 5 concludes the paper with a summary and discussion.

2. Data and methodology

Following Zhang et al. (2012), AMT is calculated with the original six-hourly spectral output of the NCAR–NCEP reanalysis (Kalnay et al., 1996) from January 1948 to December 2016, using the formula

$$\mathrm{AMT} = \iint_{\mathrm{region}} \int_{1}^{0} \frac{p_{\mathrm{s}} q v}{\rho g} d\sigma dL dt \,,$$

where p_{s} is the surface pressure, q the specific humidity, v the meridional component of the wind vector, g the gravity acceleration, ρ the density of water, and σ is the terrain-following coordinate of the data. $\int_{\mathrm{region}}$ is the longitudinal integral over the region, and $\int$ is the time integral for the selected time range.

In this study, only the AMT across the latitude of 60°N is used to measure the amount of moisture transported meridionally, in which positive numbers mean poleward transport of moisture, and negative numbers mean equatorial transport. Monthly and yearly integrations of AMT are calculated to facilitate understanding how the AMT behaves through the entire study period globally, as well as in four regions comprising North America (120°–70°W), the North Atlantic (70°W–20°E), Eurasia (20°–140°E), and the North Pacific (140°E–120°W).

The cyclone activity parameters used for this study are calculated with sea level pressure (SLP) from the same six-hourly NCEP–NCAR reanalysis for the period from January 1948 to December 2016. Then, the cyclone activity parameters between 55°N and 65°N are used to analyze and compare the relationship between cyclone activity and the AMT crossing 60°N. Selecting this area spanning 10° meridionally allows us to track, and therefore analyze, only those cyclones that developed below 60°N and crossed into the Arctic. Cyclones are identified and tracked using empirical criteria developed by Zhang et al. (2004) after examining six-hourly SLP reanalysis snapshots. The criteria used for the identification and tracking of cyclones from Zhang et al. (2004) include:

(1) If the SLP at one grid point is lower than the surround-

ing eight grid points, a cyclone candidate is identified with its center at that grid point.

(2) The minimum pressure gradient calculated between the candidate cyclone center and the adjacent eight grid points is required to be at least 0.15 hPa (100 km)$^{-1}$.

(3) The minimum SLP gradient between the cyclone candidate center and its four adjacent grid points must be negative inward for effectively removing any open lows from the data.

(4) If two or more cyclone candidates are detected within a radius of 1200 km of each other at the same time, they are considered to be a single cyclone.

(5) The cyclone candidate is required to have a minimum lifetime of 12 h. In addition, if the location of a cyclone is within 600 km of a cyclone center identified 6 h earlier, the center is considered to be a new location of the existing cyclone. Otherwise, a new cyclone is generated.

To describe the variation characteristics for cyclone activity, we use the following three cyclone activity parameters, as defined by Zhang et al. (2004):

(1) Cyclone intensity: defined by averaging the differences between the central SLP of cyclones and the climatological monthly mean SLP at corresponding grid points for all cyclones in a particular region during the month.

(2) Cyclone trajectory count (number): defined as the number of cyclones over the entire duration occurring in a particular region during the month.

(3) Cyclone Activity Index (CAI): defined as the sum of the differences between the cyclone central SLP and the climatological monthly mean SLP at corresponding grid points over all cyclone centers in a particular region during the month. Thus, CAI is an integrated parameter measuring the intensity, number and duration of cyclone activity.

3. Climatology of AMT and cyclone activity across 60°N

Performing a change-point analysis on the values of AMT that have been integrated for each year along 60°N allows us to determine whether any changes in the behavior of the data are present (Taylor, 2015). With this analysis, we identify three distinct periods at a 99% significance level by the Student's *t*-test (Fig. 1). The first period is denoted by a downward trend of −26.95 km^3 yr^{-1} of poleward yearly AMT in the first 11 years. The second period in the yearly AMT trend

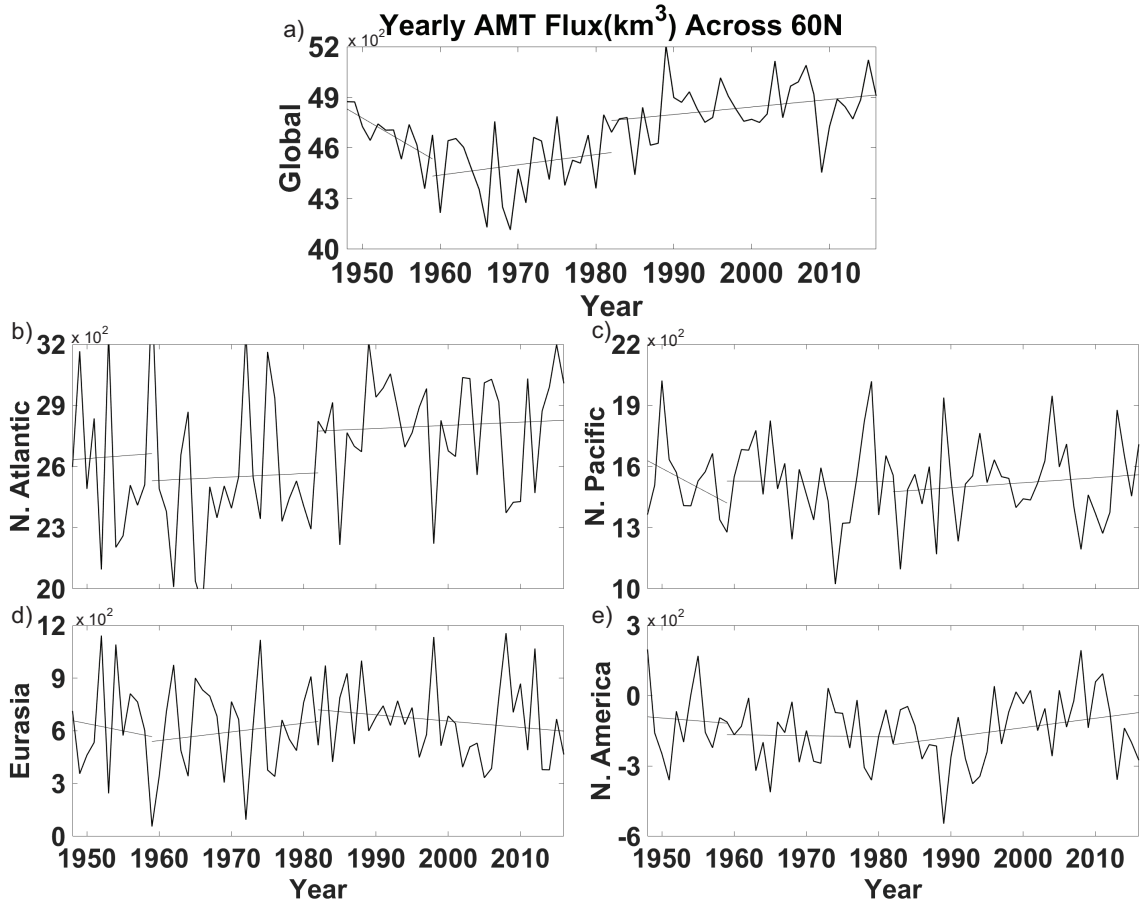

Fig. 1. Annual variation of yearly AMT (units: km^3) across 60°N (a) globally and (b–e) for the four regions of (b) the North Atlantic, (c) the North Pacific, (d) Eurasia, and (e) North America. Positive values indicate a poleward flux of moisture and negative values an equatorward flux. The thin solid straight lines are trend lines that indicate upward/downward trends for each of the three periods determined through a change-point analysis.

is identified from 1959 to 1982 where an upward trend of 6.08 km^3 yr^{-1} is present. The third and last period is defined to span from 1982 up to the end of the study period and continues the upward trend seen in the second period, albeit at a smaller magnitude of 4.46 km^3 yr^{-1}. The year 1982 marks the year in which the average of yearly AMT after 1982 is higher than the average of yearly AMT across the entire period of study, whereas the average of yearly AMT before 1982 is lower than the average yearly AMT for the period of study. Poleward yearly AMT is the largest in the North Atlantic region, followed by the North Pacific and Eurasia regions. Yearly AMT in the North America region is mainly equatorward, which was also found by Cullather et al. (2000) and Rogers et al. (2001). Annually, the yearly AMT across 60°N is 5464 km^3, in which 89% is from the oceanic regions (57% from North Atlantic and 32% from North Pacific) and 11% is from the continental regions. The Eurasia region accounts for 14% of the total poleward yearly AMT, balanced by a 3% equatorward transport in the North America region.

Using the same three periods found in the global yearly AMT (Fig. 1a) for each region (Figs. 1b–e) helps to explain the region's contributions to the trends of global yearly AMT observed in each period. During the first period, all regions except the North Atlantic present downward trends, with the North Pacific contributing to 70% of the global downward trend. For the second period, the contributions to the global upward trend are mainly provided by the North Atlantic and Eurasia. Finally, all regions except Eurasia have upward trends in the last period. Eurasia exhibiting a downward trend during this last period explains why the global upward trend is smaller than that of the second period.

Measuring the number of cyclones across 55°–65°N also demonstrates a clear regional distribution (Table 1). Annually, an average of 207 cyclones cross the latitudes of 55°–65°N, of which 66 (32%) cyclones are from the North Atlantic region and 57 (27%) from Eurasia. North America presents the smallest number with 37 (18%) cyclones, and the remaining 47 (23%) are from the North Pacific. The total cyclone number across 55°–65°N demonstrates an upward trend before 1971 and a downward trend after 1971, as indicated by the change-point analysis (Fig. 2). Similar to Zhang et al. (2004), the cyclone number in the North Pacific region exhibits a downward trend throughout both periods, which helps promote Eurasia to become a bigger contributor than the North Pacific (Table 1). In addition, Eurasia also presents the largest upward trend in cyclone number amongst all the regions for the first period.

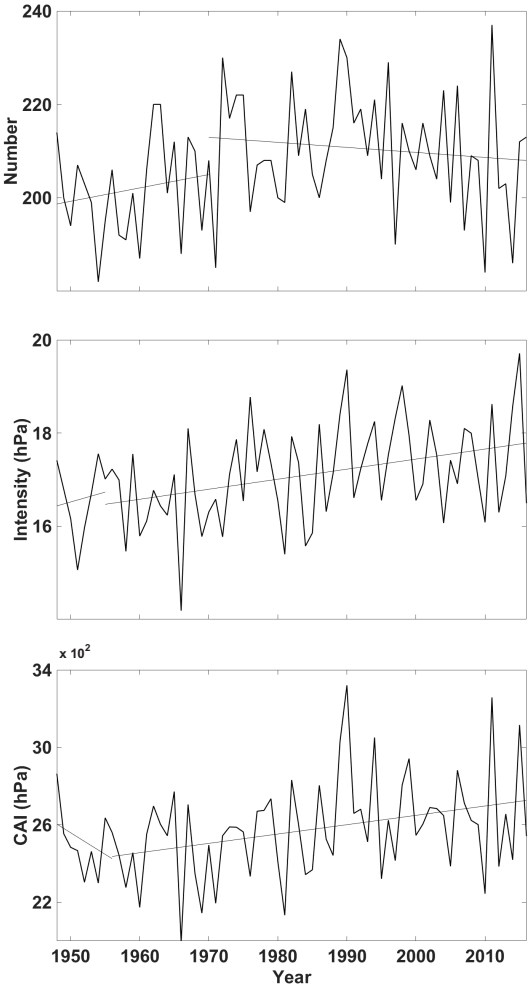

Fig. 2. Global yearly cyclone number (top), cyclone intensity (units: hPa) (middle), and CAI (units: hPa) (bottom) that crossed 60°N. The thin solid straight lines are trend lines that indicate upward/downward trends for each period determined through a change-point analysis.

Globally, the intensity of extratropical cyclones crossing 55°–65°N is around 17 hPa stronger than the mean SLP in that area (Table 1). Again, similar to Zhang et al. (2004), cyclone intensity exhibits an upward trend during the entire study period, though the change-point analysis indicates

Table 1. Cyclone number, intensity and CAI values globally and for the four regions. The percentage of the global total is provided in parentheses. For each region, trend1 and trend2 represent the trends for each period as determined from the change-point analysis and are provided in square brackets.

	Global	N. Atlantic	Eurasia	N. Pacific	N. America
Number (%)	207	66 (32%)	57 (27%)	47 (23%)	37 (18%)
[trend1; trend2]	[0.08; −0.12]	[−0.11; 0.50]	[0.36; 0.02]	[−0.25; −0.23]	[0.09; 0.04]
Intensity (hPa)	17.07	18.69	14.87	15.49	16.48
[trend1; trend2]	[0.04; 0.02]	[0.11; 0.02]	[−0.37; −0.01]	[0.22; 0.03]	[−0.23; 0.03]
CAI (%) (hPa)	2573	922 (36%)	592 (23%)	547 (21%)	512 (20%)
[trend1; trend2]	[−22.30; 4.80]	[−23.80; 2.02]	[1.60; 1.80]	[15.54; −0.72]	[−15.68; 1.73]

a slight change in the upward trend behavior in 1955 (Fig. 2). Of the various regions, we find that the North Atlantic presents the highest intensity, and the trends in each period are the closest to the global trends, which again illustrates the importance of this region to global cyclone activity (Table 1). In contrast to the trend in cyclone number, cyclone intensity in the North Pacific shows an upward trend for both periods.

Variations in cyclone number and intensity can have opposite phases; therefore, an integrated index (i.e., the CAI) is also used here to evaluate the overall variation in cyclone activity across 55°–65°N (Fig. 2). The change-point analysis is also performed for the CAI and results in a downward trend before 1956 and an upward trend after 1956. Globally, the CAI has an average of 2573 hPa across 55°–65°N, from which the most significant contributions are provided by the North Atlantic and Eurasia regions with 922 hPa (36%) and 592 hPa (23%) respectively (Table 1). The region that contributes the least to the global CAI is North America, with 512 hPa (20%). The North Pacific provides the remaining amount of 547 mb (21%), in accordance with the lower values of cyclone number and intensity when compared to the other ocean basin. Because the biggest contribution of the CAI comes from the North Atlantic region, the changes in the North Atlantic CAI throughout the study period are reflected in the global CAI. The CAI behavior during the downward trend period can be attributed to the North Atlantic and North America regions, while the upward trend period arises from the North Atlantic, Eurasia, and North America regions (Table 1). The CAI trends in the North Pacific and North America mostly cancel each other out, especially during the global downward trend period.

4. Relationship between cyclone activity and enhanced poleward AMT across 60°N

With the observed increases in both AMT and cyclone activity across 60°N and the similarity of their regional distributions, we further explore the relationship between them in this section. To understand if the trends that have been observed in AMT, as well as cyclone activity, have any relationship between one another, we calculate the trends within the distinct time series of AMT, cyclone number, cyclone intensity, and CAI. Because the observed trends are inherently long-term, a 20-yr running window is used to calculate these trends. Figures 3a–c illustrate how these trend time series behave over time. The time series of the yearly AMT trend exhibits a negative trend during 1958–67, followed by a positive trend during 1967–99. During the positive trend period, a maximum is reached around 1982, the year that the change-point analysis denotes as the beginning of the third period in the yearly AMT. The trends in cyclone number, intensity, and CAI behave differently. For example, cyclone number has a positive trend throughout the majority of the time series before 1999, while cyclone intensity begins with a relatively flat trend, then becomes negative during 1961–65, and remains positive till 1995. When the trend correlations of

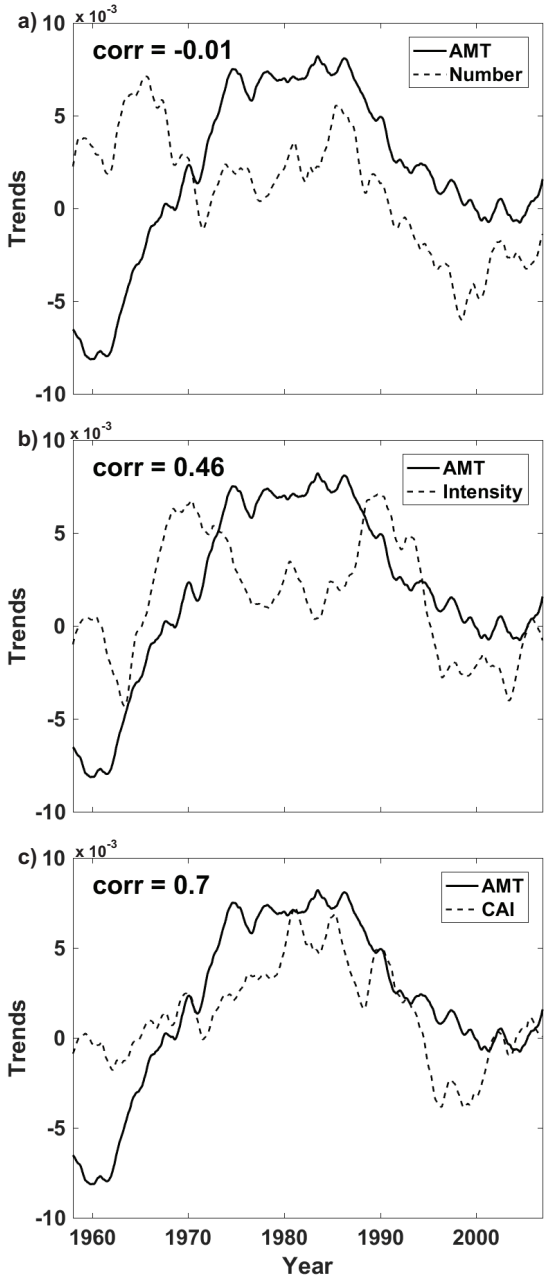

Fig. 3. Comparison of trend time series for AMT and (a) cyclone number, (b) cyclone intensity, and (c) CAI, from 1948 to 2016, using a 20-yr running window. Correlations between each variable set are shown in the plot.

yearly AMT to cyclone number, intensity, and CAI are calculated, we have −0.01, 0.46 and 0.70, respectively, of which only the latter two are significant according to the Student's *t*-test at the greater than 99% confidence level. The correlation results reveal that when the relations between cyclone activity and yearly AMT are explored, one cannot focus on simply the amount of storms or the intensity. Instead, an index such as the CAI that encompasses most major characteristics of cyclone activity including quantity, intensity, and duration is required. The trends in CAI display a similar pattern as the

trends in yearly AMT, except at the beginning of the examined period when the CAI trend is relatively flat, and during 1995–2005 when the CAI trend is negative. Therefore, the overall cyclone activity, not intensity or number only, seems to be closely related to the change in yearly AMT.

Cyclone activity, particularly in the North Atlantic, is closely tied to the AO or North Atlantic Oscillation (NAO) index. For example, a positive AO/NAO index is related to an increase in storminess in the vicinity of Iceland and the Norwegian Sea, provided by a higher amount of storms in the North Atlantic (Zhang et al., 2004; Hurrell, 2015). The variability of AMT is also well related to the AO index, mainly due to changes in the mean flow and storminess changing the moisture transport pattern (Dickson et al., 2000; Jakobson and Vihma, 2010; Hurrell, 2015). However, in recent decades, the linkage between AMT and AO, as well as the cyclone activity, have become complicated, which might be attributable to the climate pattern change from a conventional tripolar AO to an anomalous dipolar leading pattern, also known as the Arctic Rapid-change Pattern (ARP) discussed by Zhang et al. (2008).

To better understand how the atmospheric circulation pattern and associated cyclone activity impact the poleward AMT, we perform a composite analysis of SLP associated with positive and negative AMT phases. To construct the composites of SLP, plus or minus one standard deviation of monthly AMT for the month analyzed is used to group the years into when strong or weak poleward AMT is present. Figure 4 depicts the interannual variations of monthly AMT in each month. Here, we only focus on the time when the increased poleward AMT occurs, so the period with upward trends, i.e., the second and third periods (1959–2016) in the yearly AMT change-point analysis, are used to calculate the trend of monthly AMT in each month. The monthly AMT varies from month to month with greater monthly AMT (~400–500 km^3) from August to November, and weaker monthly AMT (up to ~350 km^3) from February to June. Of special interest is that from 1956 through 2016, all months show upward trends with the highest trends occurring in August (1.824 $km^3\ yr^{-1}$), September (1.297 $km^3\ yr^{-1}$), and November (1.015 $km^3\ yr^{-1}$). This suggests that any changes that affect poleward monthly AMT might be more visible in

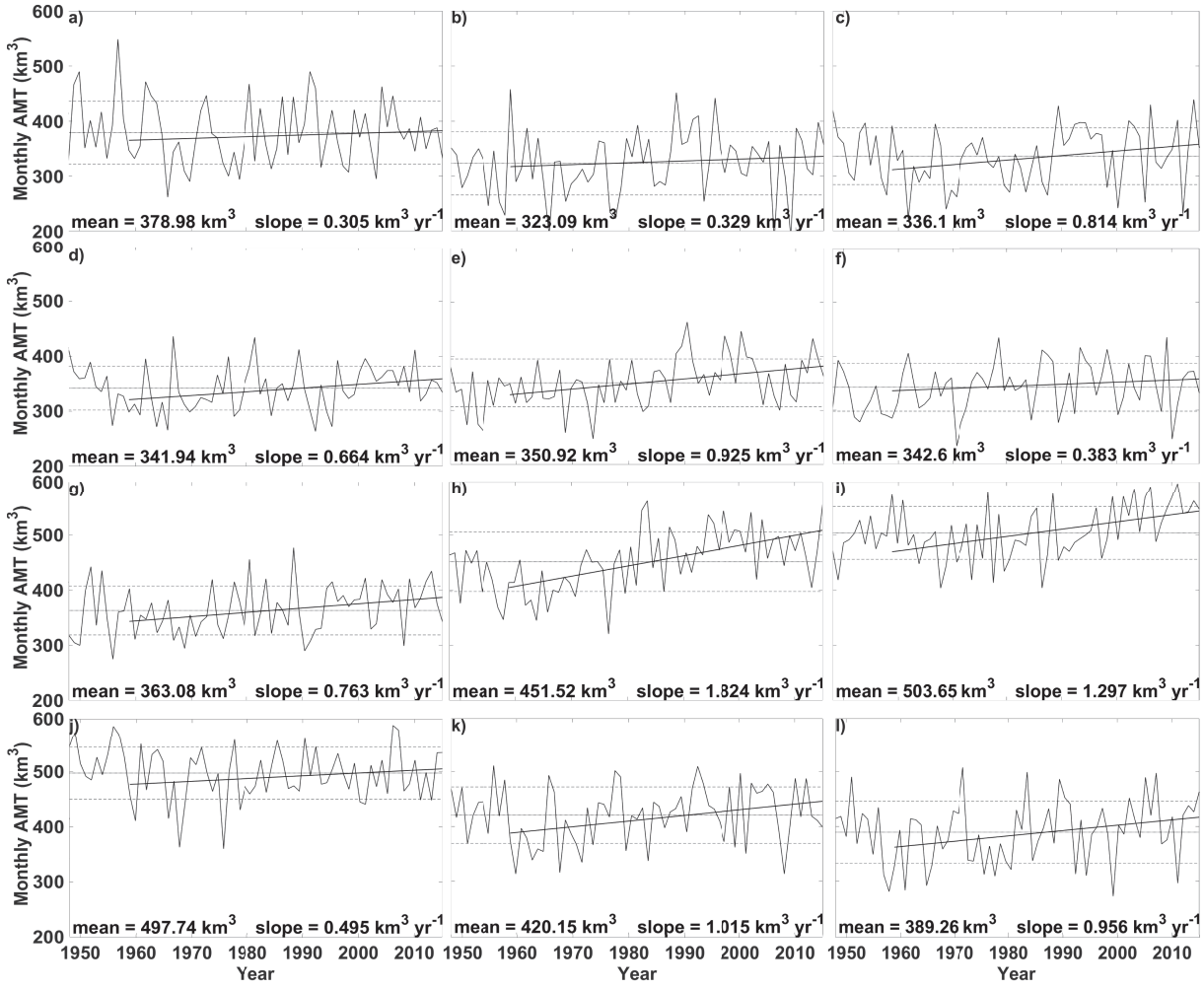

Fig. 4. Monthly AMT for (a–l) January–December, respectively, with one standard deviation above and below the mean (dotted) illustrated by dashed lines. The trend line from 1959 to 2016 is shown by a bold line.

these months. Also of interest is that October, the month with the second highest mean monthly AMT (497.74 km^3), is also one of the months with a relatively flat trend (0.495 km^3 yr^{-1}). The presence of this flat trend indicates that a relatively stable poleward monthly AMT is present in October.

The composites of SLP and monthly AMT across 60°N associated with the positive and negative AMT phases for January, April, July, and October, representative of each season, are shown in Fig. 5. During the winter month of January, we observe significant planetary-scale systems including the Siberian high, North America high, Aleutian low, and Icelandic low along the belt of 60°N (Figs. 5a and b). The differences in the SLP composites between the positive and negative phases (significant at the 99% confidence level based on the Student's *t*-test) indicate that the Icelandic low is much stronger and extends poleward into the Arctic during the positive phase. Cyclone activity crossing 60°N over the North Atlantic region, as represented by the CAI in Table 2, is also stronger during the positive phase. Enhanced poleward AMT in the North Atlantic region co-occurs with stronger cyclone activity there (Fig. 5a and Table 2).

During the spring month of April, similar differences in the SLP composite to that seen in winter are present. Again, the Icelandic low (though much weaker when compared to winter) extends poleward during the positive phase (Figs. 5d and e). Similarly, there is stronger cyclone activity crossing 60°N through the North Atlantic region co-occurring with enhanced poleward AMT in the region (Table 2).

Over summer (July), the differences in the SLP composite between the positive and negative phases are much smaller (Figs. 5g–i). The low pressure over the Arctic is slightly stronger during the positive phase. Also, the low pressure over Eurasia is slightly stronger during the negative phase. Cyclone activity crossing 60°N in the North Atlantic region is much weaker in July but still relatively strong during the positive phase (Table 2).

During fall (October), a pattern of differences in SLP composites reminiscent of that in spring and winter is again observed (Figs. 5j and k). The Icelandic low does not extend as far south as it did during the positive phase. Cyclone activity crossing 60°N measured by the CAI (Table 2) is similar to that in April, even though the entire low system is much stronger in October. During the negative phase, the Icelandic low is centered around 60°N, suggesting significant cyclone activity across there, and a relatively large CAI is observed (Table 2).

Table 2. AMT (units: km^3) and CAI (units: hPa) composite values for AMT larger than 1 standard deviation (positive phase) and smaller than 1 standard deviation (negative phase) for the North Atlantic region for January, April, July and October.

	Positive phase		Negative phase	
	AMT (km^3)	CAI (hPa)	AMT (km^3)	CAI (hPa)
January	297.75	1275.52	150.65	989.99
April	206.28	1120.70	110.74	770.63
July	243.35	714.62	205.67	514.34
October	331.09	1151.61	245.46	1038.10

Through the composite analysis performed here, it is possible to examine the relationship between the circulation pattern and associated cyclone activity and the poleward monthly AMT. Focus here is given to the North Atlantic region where the contribution to global monthly AMT is the greatest and the differences of SLP composites are significant at the 99% confidence level. A consistent relationship is found insofar as stronger cyclone activity across 60°N measured by the CAI there generally co-occurs with enhanced poleward monthly AMT in each representative seasonal month examined. This further supports why a strong correlation exists between the trends of the CAI and poleward yearly AMT.

5. Summary and discussion

The poleward AMT calculated from the NCAR–NCEP reanalysis data set has been analyzed along 60°N as a general boundary between the midlatitudes and the Arctic. An upward trend of poleward yearly AMT across 60°N since 1959 has been found, which has then consistently enhanced since 1982. The poleward yearly AMT demonstrates a distinct regional distribution, in which the maximum poleward yearly AMT occurs in the North Atlantic region. Poleward AMT also shows apparent seasonal variations, with greater values during August to November and smaller ones from February to June. An upward trend of monthly AMT is identified in all months since 1959, with the highest trend occurring in August, September, and November. It is also shown that greater poleward monthly AMT, as well as a greater upward trend, generally occurs during late summer and early fall, suggesting that the trend identified previously has continued and even amplified along with the rapidly changing Arctic system (Serreze et al., 1995; Comiso et al., 2008; Zhang et al., 2008; Skific et al., 2009).

A poleward shift in cyclone tracks has been identified by several studies (Zhang et al., 2004; Simmonds et al., 2008; Sepp and Jaagus, 2011; Bender et al., 2012), which provides an incentive to study the relationship between extratropical cyclone activity and enhanced poleward AMT. The activity of cyclones across 55°–65°N measured with cyclone number, intensity and the integrated CAI is analyzed. Similar to the upward trend in poleward yearly AMT, cyclone intensity and the CAI also demonstrate a clear upward trend since 1956, with the biggest contribution to the CAI trend coming from the North Atlantic and Eurasia regions.

The similarity of the trends observed in both the poleward yearly AMT and the activity of cyclones across 60°N motivated us to further explore the relationships between them. From the time series of linear trends constructed by using a 20-yr running window, we find a positive correlation of 0.70 between the poleward yearly AMT and CAI, an integrated measurement of cyclone activity including intensity, number, and duration. These consistent multidecadal variations be-

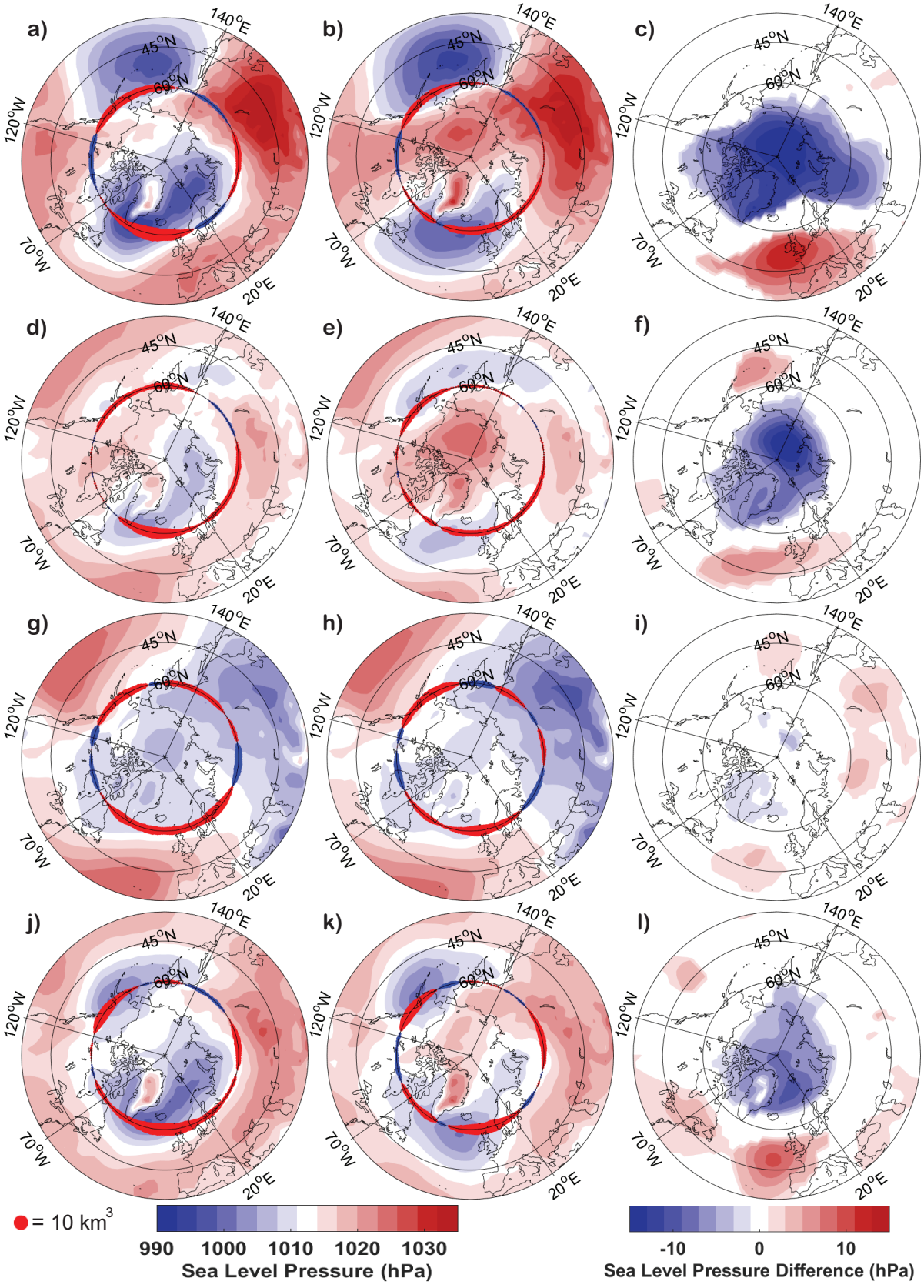

Fig. 5. Composite SLP for AMT larger than 1 standard deviation (left column) and smaller than 1 standard deviation (middle column) and their difference [right column; only statistically significant (99% confidence level) grid points plotted] for (a–c) January, (d–f) April, (g–i) July, and (j–l) October. Poleward (equatorward) moisture transport at 60°N is represented by red (blue) dots, whose sizes represent the magnitude of the transport.

tween yearly AMT and the CAI may suggest a driving role played by the overall cyclone activity in the poleward AMT, considering the fundamental nature of cyclones in holding and transporting moisture and energy.

Furthermore, a composite analysis of SLP and cyclone activity measured by the CAI and based on the positive and negative AMT phases reveals the impact of changed atmospheric circulation and cyclone activity on the poleward AMT. It is found that the poleward intrusions of the Icelandic low and accompanying enhancement of cyclone activity across 60°N would play an important role in driving the enhanced poleward AMT. The Icelandic low is generally defined on a monthly or seasonal time scale, as an integral representation of daily-scale storm activities. So, enhanced storm activity would consequently intensify the Icelandic low, perhaps through the wave breaking process. The poleward intrusion is consistent with the changes in the large-scale atmospheric circulation, which are characterized by a spatial structure shift from the AO to ARP (Zhang et al., 2008, 2012), and have decisively driven the rapid changes in the Arctic climate.

Poleward AMT impacts the Arctic climate and environment in many different ways. Since water vapor content is a major greenhouse gas, an increase in poleward AMT can thus divert moisture in the Arctic, enhancing the downward infrared radiation and, in turn, causing surface warming (e.g., Woods et al., 2013; Baggett et al., 2016; Baggett and Lee, 2017; Gong et al., 2017). In addition, a greater amount of water vapor content may lead to greater amounts of condensation, which in turn warms the atmosphere even more due to latent heat release. This may generate a positive feedback between latent heat release and the emission of atmospheric longwave radiation to the surface, further enhancing the warming and sea-ice decrease, and leading to enlarged open water and increased local evaporation. Details and quantitative analysis of this feedback process associated with cyclone activity and poleward AMT would be an appropriate avenue for follow-up research.

Acknowledgements. The authors thank the editor, Dr. Tido SEMMLER, and the anonymous reviewers, for providing insightful suggestions and comments that have greatly improved the manuscript. This work was supported by the NSF (Grant Nos. ARC-1023592, ARC-1107509, and PLR-1304684). The computing resources were provided by the Arctic Region Supercomputing Center at the University of Alaska Fairbanks.

REFERENCES

Baggett, C., and S. Lee, 2017: An identification of the mechanisms that lead to arctic warming during planetary-scale and synoptic-scale wave life cycles. *J. Atmos. Sci.*, **74**, 1859–1877, http://dx.doi.org/10.1175/JAS-D-16-0156.1.

Baggett, C., S. Lee, and S. Feldstein, 2016: An investigation of the presence of atmospheric rivers over the North Pacific during planetary-scale wave life cycles and their role in Arctic warming. *J. Atmos. Sci.*, **73**, 4329–4347, http://dx.doi.org/10.1175/JAS-D-16-0033.1.

Bender, F. A.-M., V. Ramananthan, and G. Tselioudis, 2012: Changes in extratropical storm track cloudiness 1983–2008: Observational support for a poleward shift. *Climate Dyn.*, **38**, 2037–2053, https://doi.org/10.1007/s00382-011-1065-6.

Comiso, J. C., C. L. Parkinson, R. Gersten, and L. Stock, 2008: Accelerated decline in the Arctic sea ice cover. *Geophys. Res. Lett.*, **35**, L01703, https://doi.org/10.1029/2007GL031972.

Cullather, R. I., D. H. Bromwich, and M. C. Serreze, 2000: The atmospheric hydrologic cycle over the Arctic basin from reanalyses. Part I: Comparison with observations and previous studies. *J. Climate*, **13**, 923–937, http://dx.doi.org/10.1175/1520-0442(2000)013<0923:TAHCOT>2.0.CO;2.

Dacre, H. F., P. A. Clark, O. Martinez-Alvarado, M. A. Stringer, and D. A. Lavers, 2015: How do atmospheric rivers form? *Bull. Amer. Meteor. Soc.*, **96**, 1243–1255, http://dx.doi.org/10.1175/BAMS-D-14-00031.1.

Dickson, R. R., and Coauthors, 2000: The Arctic Ocean response to the North Atlantic oscillation. *J. Climate*, **13**, 2671–2696, http://dx.doi.org/10.1175/1520-0442(2000)013<2671:TAORTT>2.0.CO;2.

Francis, J. A., and E. Hunter, 2006: New insight into the disappearing arctic sea ice. *EOS*, **87**, 509–511, http://dx.doi.org/10.1029/2006EO460001.

Gong, T. T., S. Feldstein, and S. Lee, 2017: The role of downward infrared radiation in the recent arctic winter warming trend. *J. Climate*, **30**, 4937–4949, http://dx.doi.org/10.1175/JCLI-D-16-0180.1.

Groves, D. G., and J. A. Francis, 2002: Moisture budget of the arctic atmosphere from TOVS satellite data. *J. Geophys. Res.*, **107**, ACL 11-1–ACL 11-21, http://dx.doi.org/10.1029/2001JD001191.

Guan, B., and D. E. Waliser, 2015: Detection of atmospheric rivers: Evaluation and application of an algorithm for global studies. *J. Geophys. Res.: Atmos.*, **120**, 12514–12535, http://dx.doi.org/10.1002/2015JD024257.

Hurrell, J. W., 2015: Climate variability: North Atlantic and Arctic oscillation. *Encyclopedia of Atmospheric Sciences*. 2nd ed., G. R. North et al., Eds., Elsevier Ltd., 47–60.

Jakobson, E., and T. Vihma, 2010: Atmospheric moisture budget in the Arctic based on the ERA-40 reanalysis. *International Journal of Climatology*, **30**, 2175–2194, http://dx.doi.org/10.1002/joc.2039.

Kalnay, E., and Coauthors, 1996: The NCEP/NCAR 40-year reanalysis project. *Bull. Amer. Meteor. Soc.*, **77**, 437–470, http://dx.doi.org/10.1175/1520-0477(1996)077<0437:TNYRP>2.0.CO;2.

Kay, J. E., and A. Gettelman, 2009: Cloud influence on and response to seasonal Arctic sea ice loss. *J. Geophys. Res.*, **114**, D18204, http://dx.doi.org/10.1029/2009JD011773.

Kay, J. E., T. L'Ecuyer, A. Gettelman, G. Stephens, and C. O'Dell, 2008: The contribution of cloud and radiation anomalies to the 2007 Arctic sea ice extent minimum. *Geophys. Res. Lett.*, **35**, L08503, http://dx.doi.org/10.1029/2008GL033451.

Kim, B.-M., and Coauthors, 2017: Major cause of unprecedented arctic warming in January 2016: Critical role of an Atlantic windstorm. *Scientific Reports*, **7**, 40051, http://dx.doi.org/10.1038/srep40051.

Liu, C. J., and E. A. Barnes, 2015: Extreme moisture transport into the Arctic linked to Rossby wave breaking. *J. Geophys. Res.: Atmos.*, **120**, 3774–3788, http://dx.doi.org/10.1002/2014JD022796.

Murray, R. J., and I. Simmonds, 1995: Responses of climate and

cyclones to reductions in Arctic winter sea ice. *J. Geophys. Res.*, **100**, 4791–4806, http://dx.doi.org/10.1029/94JC02206.

Newell, R. E., N. E. Newell, Y. Zhu, and C. Scott, 1992: Tropospheric rivers? —A pilot study. *Geophys. Res. Lett.*, **19**, 2401–2404, http://dx.doi.org/10.1029/92GL02916.

Newman, M., G. N. Kiladis, K. M. Weickmann, F. M. Ralph, and P. D. Sardeshmukh, 2012: Relative contributions of synoptic and low-frequency eddies to time-mean atmospheric moisture transport, including the role of atmospheric rivers. *J. Climate*, **25**, 7341–7361, http://dx.doi.org/10.1175/JCLI-D-11-00665.1.

Peixoto, J. P., and A. H. Oort, 1992: *Physics of Climate*. American Institute of Physics, 520 pp.

Ralph, F. M., and M. D. Dettinger, 2011: Storms, floods, and the science of atmospheric rivers. *EOS*, **92**, 265–266, http://dx.doi.org/10.1029/2011EO320001.

Rogers, A. N., D. H. Bromwich, E. N. Sinclair, and R. I. Cullather, 2001: The atmospheric hydrologic cycle over the Arctic basin from reanalyses. Part II: Interannual variability. *J. Climate*, **14**, 2414–2429, http://dx.doi.org/10.1175/1520-0442(2001)014<2414:TAHCOT>2.0.CO;2.

Sepp, M., and J. Jaagus, 2011: Changes in the activity and tracks of arctic cyclones. *Climatic Change*, **105**, 577–595, http://dx.doi.org/10.1007/s10584-010-9893-7.

Serreze, M. C., R. G. Barry, and J. E. Walsh, 1995: Atmospheric water vapor characteristics at 70°N. *J. Climate*, **8**, 719–731, http://dx.doi.org/10.1175/1520-0442(1995)008<0719:AWVCA>2.0.CO;2.

Simmonds, I., and K. Keay, 2009: Extraordinary September Arctic sea ice reductions and their relationships with storm behavior over 1979–2008. *Geophys. Res. Let.*, **36**, L19715, http://dx.doi.org/10.1029/2009GL039810.

Simmonds, I., C. Burke, and K. Keay, 2008: Arctic climate change as manifest in cyclone behavior. *J. Climate*, **21**, 5777–5796, http://dx.doi.org/10.1175/2008JCLI2366.1.

Skific, N., J. A. Francis, and J. J. Cassano, 2009: Attribution of projected changes in atmospheric moisture transport in the Arctic: A self-organizing map perspective. *J. Climate*, **22**, 4135–4153, http://dx.doi.org/10.1175/2009JCLI2645.1.

Sorteberg, A., and B. Kvingedal, 2006: Atmospheric forcing on the Barents Sea winter ice extent. *J. Climate*, **19**, 4772–4784, http://dx.doi.org/10.1175/JCLI3885.1.

Taylor, W. A., 2015: Change-Point Analysis: A powerful new tool for detecting changes. Taylor Enterprises., [Available online from http://www.variation.com/cpa/tech/changepoint.html]

Thompson, D. J. W., and J. M. Wallace, 1998: The Arctic oscillation signature in the wintertime geopotential height and temperature fields. *Geophys. Res. Lett.*, **25**, 1297–1300, http://dx.doi.org/10.1029/98GL00950.

Vihma, T., and Coauthors, 2016: The atmospheric role in the Arctic water cycle: A review on processes, past and future changes, and their impacts. *J. Geophys. Res.: Biogeosci.*, **121**, 586–620, http://dx.doi.org/10.1002/2015JG003132.

Wang, X. J., and J. R. Key, 2005: Arctic surface, cloud, and radiation properties based on the AVHRR polar pathfinder dataset. Part II. Recent trends. *J. Climate*, **18**, 2575–2593, https://doi.org/10.1175/JCLI3439.1.

Woods, C., and R. Caballero, 2016: The role of moist intrusions in winter Arctic warming and sea ice decline. *J. Climate*, **29**, 4473–4485, http://dx.doi.org/10.1175/JCLI-D-15-0773.1.

Woods, C., R. Caballero, and G. Svensson, 2013: Large-scale circulation associated with moisture intrusions into the Arctic during winter. *Geophys. Res. Lett.*, **40**, 4717–4721, http://dx.doi.org/10.1002/grl.50912.

Yin, J. H., 2005: A consistent poleward shift of the storm tracks in simulations of 21st century climate. *Geophys. Res. Lett.*, **32**, L18701, http://dx.doi.org/10.1029/2005GL023684.

Zhang, X. D., J. E. Walsh, J. Zhang, U. S. Bhatt, and M. Ikeda, 2004: Climatology and interannual variability of Arctic cyclone activity: 1948–2002. *J. Climate*, **17**, 2300–2317, http://dx.doi.org/10.1175/1520-0442(2004)017<2300:CAIVOA>2.0.CO;2.

Zhang, X. D., A. Sorteberg, J. Zhang, R. Gerdes, and J. C. Comiso, 2008: Recent radical shifts of atmospheric circulations and rapid changes in Arctic climate system. *Geophys. Res. Lett.*, **35**, L22701, http://dx.doi.org/10.1029/2008GL035607.

Zhang, X. D., J. X. He, J. Zhang, I. Polyakov, R. Gerdes, J. Inoue, and P. L. Wu, 2012: Enhanced poleward moisture transport and amplified northern high-latitude wetting trend. *Nat. Clim. Change*, **3**, 47–51, http://dx.doi.org/10.1038/nclimate1631.

Zhu, Y., and R. E. Newell, 1998: A proposed algorithm for moisture fluxes from atmospheric rivers. *Mon. Wea. Rev.*, **126**, 725–735, http://dx.doi.org/10.1175/1520-0493(1998)126<0725:APAFMF>2.0.CO;2.

Zuidema, P., and Coauthors, 2005: An Arctic springtime mixed-phase cloudy boundary layer observed during SHEBA. *J. Atmos. Sci.*, **62**, 160–176, http://dx.doi.org/10.1175/JAS-3368.1.